MnO_2/Carbon Nanofibers Material as High Performance Anode for Lithium-Ion Batteries

Dandan Ma , Xin Mu , Guiqing Zhao , Xiangge Qin * , Meili Qi *

Posted Date: 21 March 2023

doi: 10.20944/preprints202303.0359.v1

Keywords: lithium-ion batteries, Carbon nanofibers, MnO2, the anode material

Article

MnO_2/Carbon Nanofibers Material as High Performance Anode for Lithium-Ion Batteries

Dandan Ma [1,2], Xin Mu [1], Guiqing Zhao [1], Xiangge Qin [1,*] and Meili Qi [1,*]

[1] School of Materials Science and Engineering, Jiamusi University, Jiamusi 154007, China
[2] School of Information Science and Electronic Technology, Jiamusi University, Jiamusi 154007, China
* Correspondence: qinxiangge@jmsu.edu.cn (X.Q.); meili8585@foxmail.com (M.Q.); Tel.: +86-04548618703

Abstract: High-performance anodes are contributed to nanostructure of transition metal oxides for rechargeable Li-ion batteries (LIBs). In this work, we report the fabrication of high-performance anode materials for lithium-ion batteries, MnO_2 nanotube directly grown into fabrics of carbon nanofibers, the MnO_2/Carbon nanofibers (CNFs) were investigated by X-ray diffraction, scanning and transmission electron microscopies. When tested as the anode material in LIBs, the MnO_2/CNFs exhibit superior performance and excellent long cycling performance with a reversible capacity of 835 mA h g^{-1} at 0.1 A g^{-1} after the 133 th cycle, a high initial specific capacity of 1094 mA h g^{-1} at a current density of 0.1 A g^{-1}. The MnO_2/CNFs demonstrates notable specific capacities, specifically, with a coulombic efficiency of 99.5 %, both stability and capacity are conspicuously above literature data. These impressive results indicate that MnO_2/CNFs has great potential for high-energy and high-power energy storage applications.

Keywords: lithium-ion batteries; carbon nanofibers; MnO_2; the anode material

1. Introduction

Rechargeable lithium-ion batteries are the critical energy storage devices over the last decades, they have been regarded as the first choice for electric automobile, portable electronics because of their high energy density, durable cycle life and eco-friendly [1–3]. Electrode materials, especially anodes, they are very important components of LIBs, may play a decisive role in the whole performances [4–6]. Up to now, the graphite is still considered as the most common used anode materials in large amounts of LIBs, in fact it is subjected to the low specific capacity (372 mA h g^{-1}), which severely limited the application of LIBs [6–8]. Thus, researchers continue to explore advanced anode materials, that it could replace of the graphite [9–12].

Various transition metal oxides (TMOs) have paid much attention due to their excellent electrochemical properties [13–18]. Among of them, manganese oxides are considered as one of the most potential anode materials for high theoretical energy, owing to its low price, high theoretical capacity, variety of crystal structures and environmental friendliness (e.g., MnO_2, MnO, Mn_2O_3, and Mn_3O_4) [19–21]. However, manganese oxide anodes also have many disadvantages, involving volume change during the process of charge/discharge repeatedly and poor electrical conductivity, which result in poor rate capacity and inferior cycling stability [22,23]. To solve the problems and improve the electrochemical performance, many effective strategies have been researched, for instance, materials [24], porous structure, conductive polymers/ metallic materials coating [25–28].

Sui *et al.* illustrated semiconducting polypyrrole coated-δ-MnO_2 nanosheet arrays on nickel foam (denoted as MnO_2@PPy/NF) are prepared via hydrothermal growth of MnO_2 followed by the electrodeposition of PPy on the anode in LIBs. The electrode with ~50 nm thick PPy coating exhibits an outstanding overall electrochemical performance [29]. Lin *et al.* showed MnO/C cubo-polyhedrons were successfully constructed with carbonizing α-MnO_2@ZIF-8 precursors synthesized using sea urchin shaped α-MnO_2 microspheres as a template. The as-prepared samples possess an irregular polyhedral cubic structure matrix coated with a thin carbon layer, which has the outstanding long cycling performance with a reversible capacity [30]. Cao *et al.* demonstrated hollow carbon nanospheres (HCN) loaded with MnO_2 (denoted as MnO_2@HCN) are investigated as an anode

 doi:10.20944/preprints202303.0359.v1

material for lithium-ion batteries. HCN is developed by treatment of 3-aminophenol and formaldehyde resin. MnO_2 is loaded on the outer surface of HCN via the reduction of $KMnO_4$ to form porous core-shell structures. SEM, TEM and XRD characterizations indicate that the MnO_2@HCN has a spherical morphology with a core consisting of porous carbon nanoparticles and a shell consisting of MnO_2 nanoparticles [31].

In this document, MnO_2 was firstly synthesized through the hydrothermal, then MnO_2 nanotubes (NTs) were obtained by calcination in air. Add to polyacrylonitrile (PAN) particles after MnO_2 nanotubes mixed with the dimethylformamide, using heat treatment and electrospinning, and finally the MnO_2/Carbon nanofibers (CNFs) was prepared. This material demonstrates the high specific capacity and the retention rate, outstanding performance of long cycling, and the excellent stability.

2. Experimental

2.1. Preparation of MnO_2

The transition metal Oxide MnO_2 was prepared by hydrothermal method. Firstly, 0.2 g $KMnO_4$ was mixed with 25 mL H_2O and stirred for 10 minutes. Then, 1.25 mL HNO_3 was added and fully stirred and transferred to a 50 mL Teflon lined stainless steel reactor for hydrothermal reaction at 120 °C for 12 h, natural cooling, centrifugal washing at 10000 rates, and then dry. MnO_2 powder was prepared.

2.2. Preparation of MnO_2 NTs

MnO_2 was calcined to produce MnO_2 NTs. MnO_2 powder was placed in a tubular furnace and placed in 400°C air for 4 hours for heat treatment to obtain MnO_2 NTs.

2.3. Preparation of MnO_2 Nanofibers (NFs)

The polymer containing 5% MnO_2 NFs and 20% MnO_2 NFs were prepared by electrospinning. Weighing out the required of MnO_2 NTs, respectively , and N,N dimethylformamide (Tianjin Kaitong Chemical Reagent Co., LTD.) mixed, put in the ultrasonic cleaning machine fully dissolved, then add the appropriate amount of polyacrylonitrile (PAN), continue to put in the ultrasonic cleaning machine until all dissolved, mixed into the required slurry into the electrostatic spinning machine for spinning. After re-coating by electrospinning, containing the polymer of 5% MnO_2 NFs and 20% MnO_2 NFs were prepared.

2.4. Preparation of MnO_2 /CNFs

MnO_2 NFs polymer was calcined to produce MnO_2/CNFs. 5% MnO_2 NFs polymer and 20% MnO_2 NFs polymer were placed in tubular furnace respectively and carbonized in Ar atmosphere at 600°C for 4 hours to obtain 5% MnO_2/CNFs and 20% MnO_2/CNFs (Figure 1).

Preprints (www.preprints.org) | NOT PEER-REVIEWED | Posted: 21 March 2023 doi:10.20944/preprints202303.0359.v1

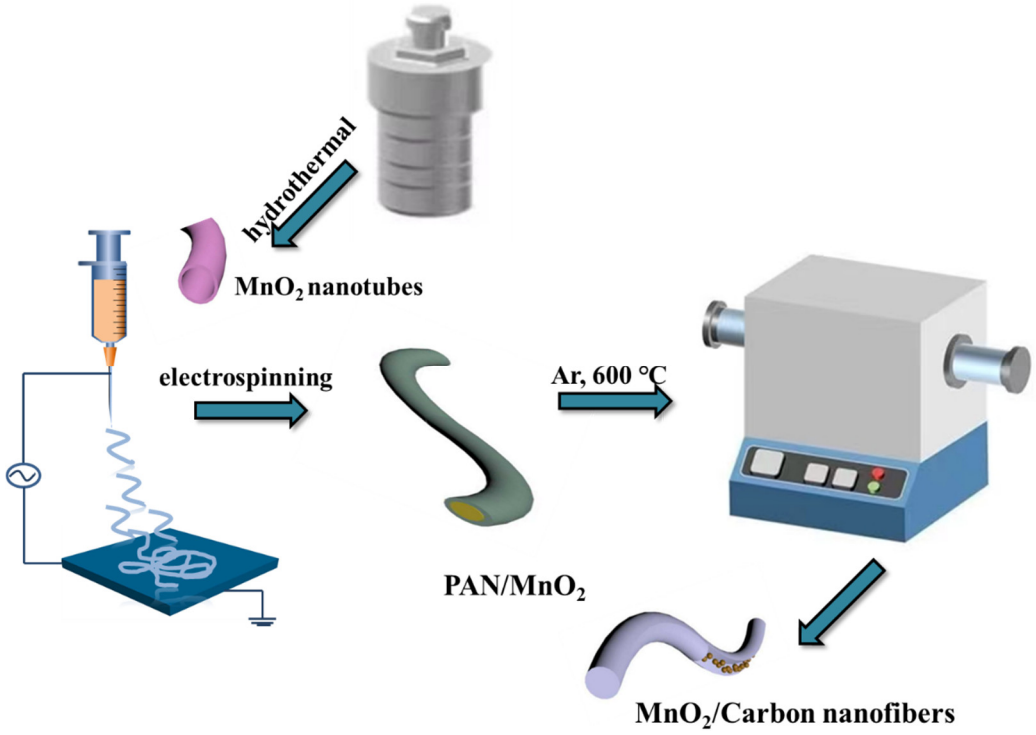

Figure 1. Schematic of the synthesis procedure of the MnO_2/Carbon nanofibers.

2.5. Materials Characterization

The composition of MnO_2 NTs, 5% MnO_2/CNFs and 20% MnO_2/CNFs were characterized by X-ray diffractometry (XRD, D8Advance, Bruker AXS, Germany), scanning electron microscope (SEM, JSM-6360LV, JEOL, Japan) and transmission electron microscope (TEM, Fei Tecnai G2 F20S-Twin) were used to further observe the morphology of the tissue. The batteries were assembled in the glove box. 5 % MnO_2/CNFs and 20 % MnO_2/CNFs were selected as anode materials, and dry at room temperature for 24 h.

3. Results and Discussion

3.1. Morphology and Structure

The morphology and structure images of MnO_2 NTs, 5 % MnO_2 /CNFs and 20 % MnO_2 /CNFs were obtained. Figure 2 characterizes the morphology of MnO_2 NTs by scanning electron microscopy (SEM) at different magnifications. Figure 2a displays the tubular structure of MnO_2 NTs with the longest of about 3.3 μm, the morphologies of MnO_2 NTs have better uniformity, have almost no impurity particles. As shown in Figure 3b, hollow tubes are gained with an average diameter of 100 nm (±100). Figure 3a,b show that the 5 % MnO_2/CNFs, and 3c-d show the 20 % MnO_2/CNFs, both of them are the uniform nanofiber with a diameter of approximately 300–500 nm, and uniformly distributed nanoparticles are in the high component, it reveals that the uniform MnO_2/CNFs can be prepared [32,33].

Preprints (www.preprints.org) | NOT PEER-REVIEWED | Posted: 21 March 2023 doi:10.20944/preprints202303.0359.v1

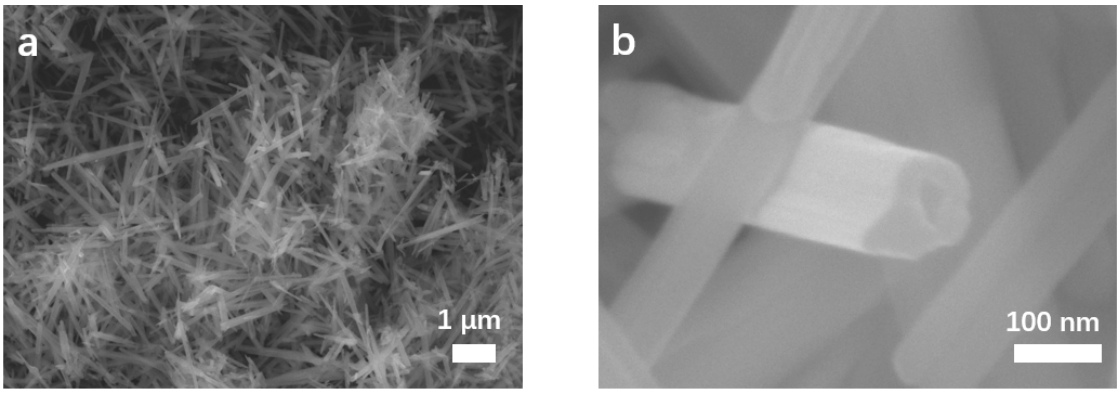

Figure 2. SEM images of MnO_2 NTs (**a**,**b**).

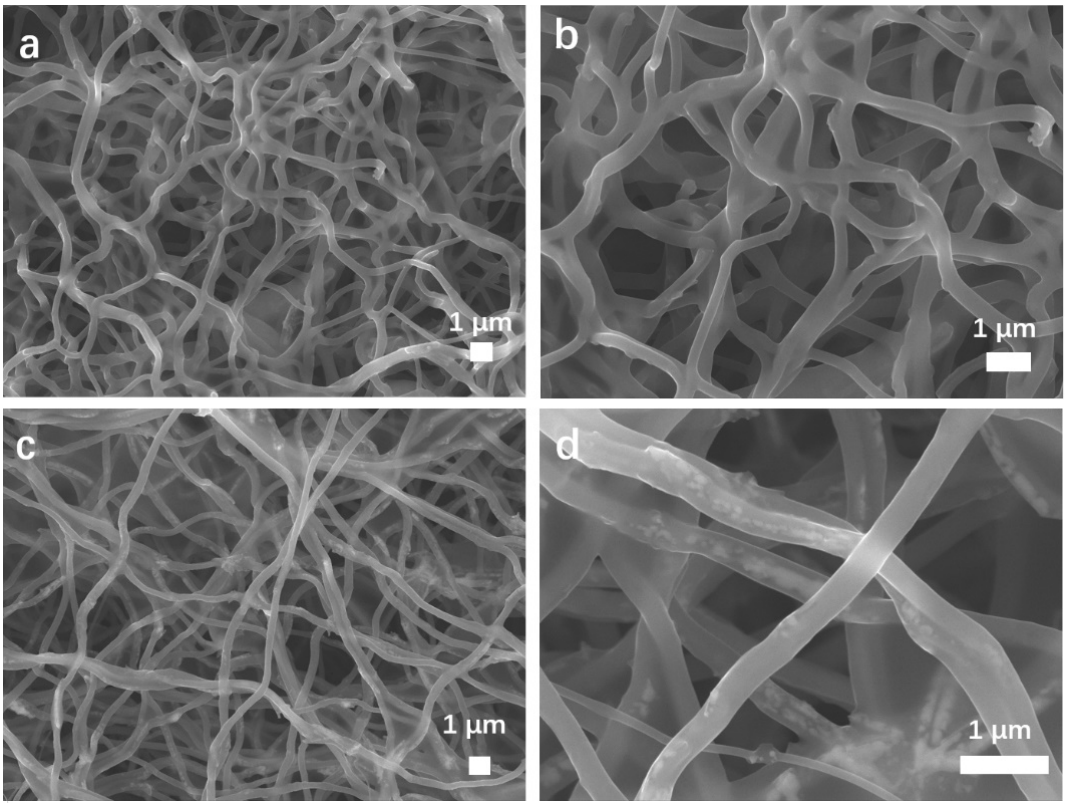

Figure 3. SEM images of the MnO_2/CNFs at different components: 5 % MnO_2/CNFs (**a**,**b**); 20 % MnO_2/CNFs (**c**,**d**).

The crystal structures and phase information of MnO_2 NTs, 5 % MnO_2/CNFs and 20 % MnO_2/CNFs were characterized by X-ray powder diffraction (XRD), the results are demonstrated in Figure 4, the diffraction peaks of MnO_2 NTs, 5 % MnO_2/CNFs and 20 % MnO_2/CNFs are in line with the standard card of MnO_2 (JCPDS NO. 44-0141), the XRD patterns of MnO_2 NTs, 5 % MnO_2/CNFs and 20 % MnO_2/CNFs show no noticeable change. The typical diffraction peaks correspond to the (110), (200), (220), (310), (211), (301), (411), (431), (521), (002), (541), (312) and (332) crystal planes of manganese dioxide, respectively. This indicated that manganese dioxide was integrate into the composite material, which present the successful preparation. The peak of 20 % MnO_2/CNFs is strong and narrow, confirmed that the good crystallinity and high purity [34,35].

Preprints (www.preprints.org) | NOT PEER-REVIEWED | Posted: 21 March 2023 doi:10.20944/preprints202303.0359.v1

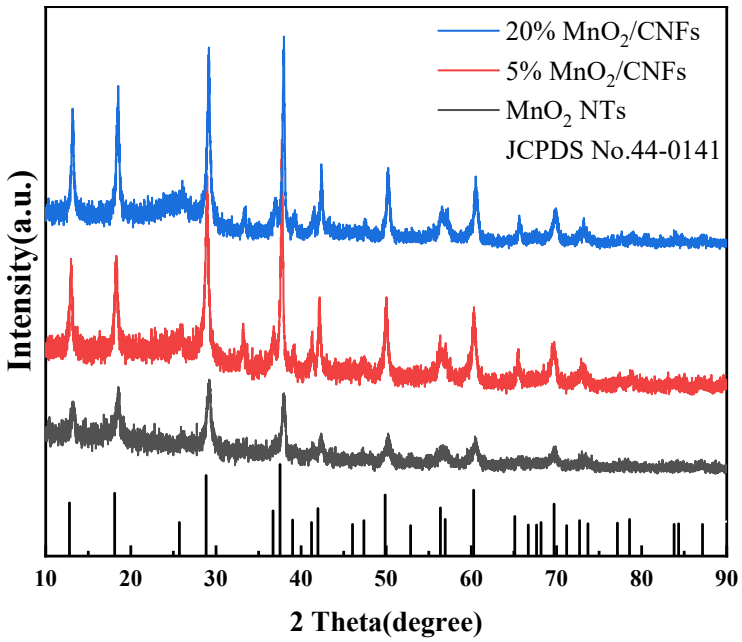

Figure 4. XRD patterns of MnO_2 NTs, 5 % MnO_2/ CNFs and 20 % MnO_2/ CNFs.

In order to obtain further investigation into the structure of 20 % MnO_2/CNFs samples, TEM characterization is carried out in Figure 5. The prepared 20 % MnO_2/CNFs showed a nanotube structure with the diameter of 250 nm which is filled with the MnO_2 particles in Figure 5b. In Figure 5c, the high resolution TEM image of the MnO_2/CNFs exhibits that the lattice spacings are 0.182 nm and 0.161 nm, which are consistent with the spacing of the (411) and (431) planes of MnO_2, obviously, demonstrating the composition of the nanofibers to be MnO_2 again [35–37].

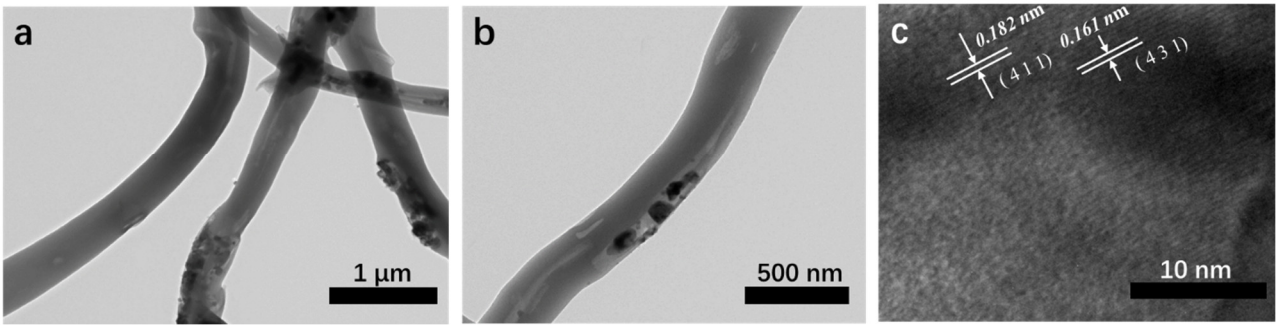

Figure 5. TEM images of 20% MnO_2 /CNFs (**a**,**b**) and HRTEM image of 20% MnO_2 /CNFs (**c**).

3.2. Electrochemical Performance

The lithium electrochemical performance of MnO_2 NTs, 5 % MnO_2/CNFs and 20 % MnO_2/CNFs were evaluated using coin cells. The CV curves of MnO_2 NTs, 5 % MnO_2/ CNFs and 20 % MnO_2/ CNFs for the first several cycles at a scan rate of 0.1 mV s^{-1} in the potential range 0.01-3.0 V, respectively, in Figure 6a–c. Compared with MnO_2 NTs and 5 % MnO_2/CNFs in Figure 6a,b, in the first cathodic cycle creates a broad peak at 0.45 V in Figure 6c, which vanishes in the following cathodic cycles, it illustrates that the reaction is irreversible and the energy difference prompts the formation of the solid electrolyte interface (SEI) on the electrode surface [30,31]. In addition to this, a peak decreases sharply below 0.35 V is because of the reduction of Mn^{4+} to Mn^0 ($MnO_2 + 4Li^+ + 4e^- \rightarrow Mn + 2Li_2O$) [30,38]. In the first anodic cycles, the strong peak at 1.32 V is corresponding to the dissolution of Li^+ from Li_2O and the oxication of Mn^0 to Mn^{2+} ($Mn + 2Li_2O \rightarrow MnO_2 + 4Li^+ + 4e^-$) [30,31,38]. In the other anodic cycles, the reaction is reversible because of the peaks have no obvious changes and almost in the same place, the excellent electrochemical stability was revealed.

Preprints (www.preprints.org) | NOT PEER-REVIEWED | Posted: 21 March 2023 doi:10.20944/preprints202303.0359.v1

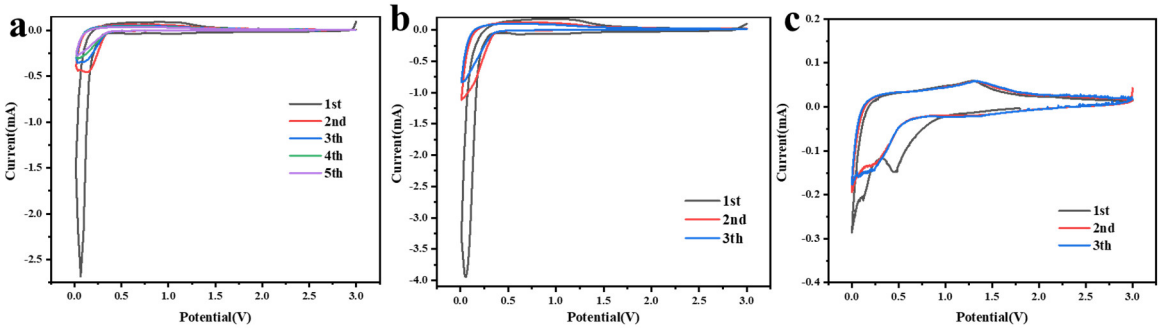

Figure 6. Cyclic Voltammetry curves of MnO_2 NTs (**a**), 5 % MnO_2/ CNFs (**b**) and 20 % MnO_2/ CNFs (**c**) at a scan rate of 0.1 mV s^{-1} in the potential range 0.01-3.0 V.

The discharge/charge graph of 5 % MnO_2/ CNFs and 20 % MnO_2/ CNFs at a current density of 0.1Ag^{-1} are displayed in Figure 7a,b. The curves of lap 1, lap 20 and lap 50 were regarded as the samples, there is an obvious discharge voltage plateaus at about 0.76V (Figure 7a) and 0.57V (Figure 7b), the specific capacity of the first discharge are 1023 mA h g^{-1} and 1094 mA h g^{-1}, respectively, the following cycles, the specific capacity are around 531-558 mA h g^{-1} and 658-704 mA h g^{-1}, an SEI film was formed due to the lost capacity, which is irreversible, it is the same as cyclic voltammetry curves (Figure 7a,b), the mechanism of alloying lithiation is proved. Meanwhile, the discharge/charge capacity of the 20% MnO_2/CNFs remain higher than the 5% MnO_2/CNFs, it is indicated that not only the high performance, but also the excellent battery reversibility [39,40].

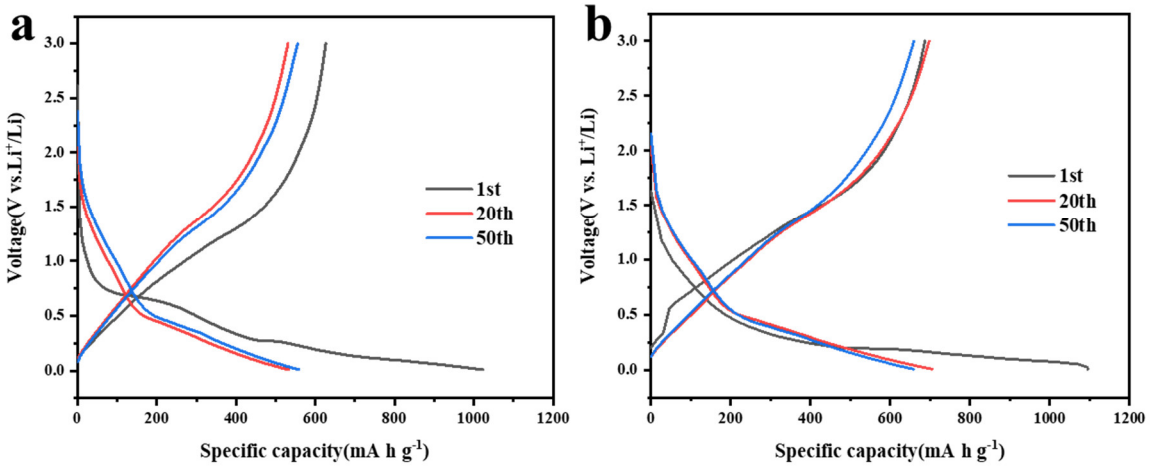

Figure 7. Discharge/charge curves in selected cycles for 5 % MnO_2/ CNFs (**a**) and 20 % MnO_2/ CNFs (**b**).

The cycling performance of 5 % MnO_2/CNFs for 160 cycles and 20 % MnO_2/CNFs for 200 cycles at a current density of 0.1 A g^{-1} are shown in Figure 8a,b. The initial discharge/charge specific capacities of 20 % MnO_2/CNFs are 1094 mA h g^{-1} and 687 mA h g^{-1}, higher than 5 % MnO_2/CNFs. By the cycles continues, the specific capacities 5 % MnO_2/CNFs maintains at around 610 mA h g^{-1} from the 117 th cycle to the 160 th cycle, while 20 % MnO_2/CNFs remains at around 835 mA h g^{-1} from the133 th cycle to the 200 th cycle. During the whole process, coulombic efficiency of them hold at around 98.9 % and 99.5 %, respectively, 20 % MnO_2/CNFs owns the higher coulombic efficiency obviously, these confirm that the more percentage of MnO_2/CNFs, the better reversibility and structural stability [41–43].

Preprints (www.preprints.org) | NOT PEER-REVIEWED | Posted: 21 March 2023 doi:10.20944/preprints202303.0359.v1

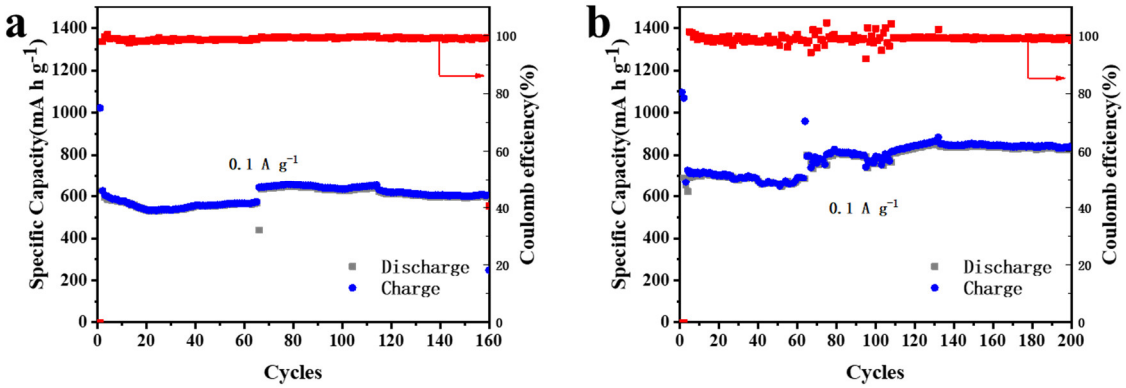

Figure 8. Cycling performance of 5 % MnO_2/CNFs for 160 cycles (**a**) and 20 % MnO_2/CNFs for 200 cycles (**b**) at a current density of 0.1 A g^{-1}.

To compare the discharge/charge capacity, the rate performance of MnO_2 NTs, 5 % MnO_2/CNFs and 20 % MnO_2/CNFs are tested at various current rates ranging from 0.1 to 0.5 A g^{-1} (Figure 9a–c). MnO_2 NTs does not contain the MnO_2/CNFs in it, so the structure is damaged easily and the cycle is unstable (Figure 9a). On the contrary, because of the carbon nanofibers, 5 % MnO_2/CNFs and 20 % MnO_2/CNFs have the good structural stability (Figure 9b,c), but 20 % MnO_2/CNFs show the superior capacity, the corresponding invertible capacities are 796, 611, 552, 486 mA h g^{-1} at 0.1, 0.2, 0.3, 0.5 A g^{-1}. When test again at 0.1, 0.2, 0.3 A g^{-1}, the reversible capacity of 835, 620,565 mA h g^{-1} are reached. In addition, the MnO_2/CNFs shows better rate capability compared to the MnO_2 NTs nanoparticle electrode at various rates from 0.1 to 0.5 A g^{-1} (Figure 9).

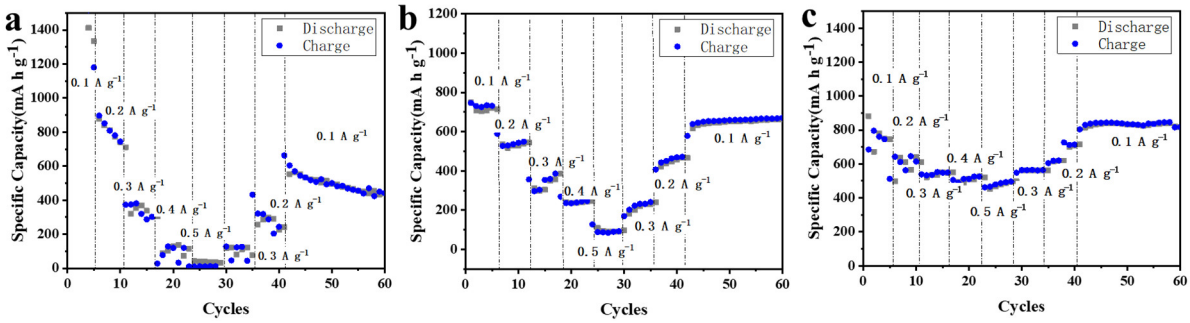

Figure 9. Rate performance of MnO_2 NTs (**a**), 5% MnO_2/ CNFs (**b**) and 20% MnO_2/ CNFs (**c**) at various current rates ranging from 0.1 to 0.5Ag^{-1}.

3.3. Analysis of Electrode Structure after Circulation

In order to further prove the relationship between the fiber structure and the cycling stability, the electrode was disassembled after the cycling, the structure and morphology are shown in Figure 10. It is very clearly to see that 20 % MnO_2/CNFs still maintain the fiber structure, and the fiber structure is not broken, the porous fiber can release the expanded volume of the alloy effectively during the lithium process, thus maintaining the stability of the structure and improving the stability and efficiency of the cycle.

 doi:10.20944/preprints202303.0359.v1

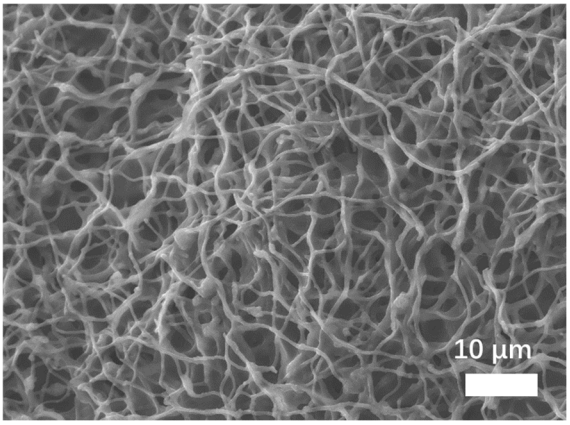

Figure 10. SEM images of the 20% MnO_2/CNFs after 200 cycles.

4. Conclusions

This study provides a simple method to prepare MnO_2/CNFs material as high performance anode, MnO_2/CNFs were prepared by electrospinning, the electrochemical properties of MnO_2 NTs, 5 % MnO_2/CNFs and 20 % MnO_2/CNFs are evaluated. Comparison with them, 20 % MnO_2/CNFs anode can provide the initial reversible capacity of 1094 mA h g^{-1} at 0.1 mA g^{-1} and remains 835 mA h g^{-1} after 133 cycles. The results show that 20 % MnO_2/CNFs had better the good structural stability, high specific capacity, excellent reversibility, the long cycling performance, and superior ionic conductivity, which provided ideas and prospect for designing a high performance anode for LIBs.

Acknowledgments: The authors acknowledge financial support from Fundamental Research Funds for the Central Universities of Heilongjiang Province of China (2022-KYYWF-0603), Research Fund for the Doctoral Program of Higher Education of China (JMSUBZ 2020-02) and Fundamental Research Funds for the Central Universities of Heilongjiang Province of China (2021-KYYWF-0554).

Conflicts of Interest: The authors declare that they have no known competing financial interests or personal relationships that could have appeared to influence the work reported in this paper.

References

1. Takeuchi; E.S.; Takeuchi; K.J.; Marschilok, A.C. The Ongoing Importance of Lithium Primary Batteries: 50+ Years and Going Strong. *ECS Meet. Abstr.* **2022**, *MA2022-02*, 102.
2. Zheng; Y.; Yao; Y.; Ou; J.; Li; M.; Luo; D.; Dou; H.; Li; Z.; Amine; K.; Yu; A.; Chen, Z. A review of composite solid-state electrolytes for lithium batteries: Fundamentals, key materials and advanced structures. *Chem. Soc. Rev.* **2020**, *49*, 8790–8839.
3. Zeng; X.; Li; M.; El-Hady; D.A.; Alshitari; W.; Al-Bogami; A.S.; Lu; J.; Amine, K. Commercialization of lithium battery technologies for electric vehicles. *Adv. Energy Mater.* **2019**, *9*, 1900161.
4. Evarts, E.C. Lithium batteries: To the limits of lithium. *Nature* **2015**, *526*, S93–S95.
5. Y.; Chen; W.; Lei; T.; Jiao; Y.; Huang; J.; Hu; A.; Gong; C.; Yan; C.; Wang; X.; Xiong, J. Strategies toward high-loading lithium–sulfur battery. *Adv. Energy Mater.* **2020**, *10*, 2000082.
6. Roselin; L.S.; Juang; R.-S.; Hsieh; C.-T.; Sagadevan; S.; Umar; A.; Selvin; R.; Hegazy, H.H. Recent Advances and Perspectives of Carbon-Based Nanostructures as Anode Materials for Li-ion Batteries. Materials **2019**, *12*, 1229.
7. X.; Zhang; M.; Yuan; S.; Lu, C. Research Progress of Silicon/Carbon Anode Materials for Lithium-Ion Batteries: Structure Design and Synthesis Method. *ChemElectroChem* **2020**, *7*, 4289–4302.
8. Y.; Chen, J. Prospects of organic electrode materials for practical lithium batteries. *Nat. Rev. Chem.* **2020**, *4*, 127–142.
9. Luo; J.; Peng; J.; Zeng; P.; Wu; Z.; Li; J.; Li; W.; Huang; Y.; Chang; B.; Wang, X. TiNb2O7 nano-particle decorated carbon cloth as flexible self-support anode material in lithium-ion batteries. *Electrochim. Acta* **2019**, *332*, 135469.
10. Kim; H.; Choi; W.; Yoon; J.; Lee; E.; Yoon, W.S. Polymorphic Effects on Electrochemical Performance of Conversion-Based MnO2 Anode Materials for Next-Generation Li Batteries. *Small* **2021**, *17*, 2006433.

11. C.; Li; C.; Tang; H.; Liu; T.; Tang, Z. Binder-free flexible Li2ZnTi3O8@MWCNTs stereoscopic network as lightweight and superior rate performance anode for lithium-ion batteries. *J. Alloy. Compd.* **2019**, *816*, 152580.
12. Chen; Y.; Yuan; X.; Yang; C.; Lian; Y.; Razzaq; A.A.; Shah; R.; Guo; J.; Zhao; X.; Peng; Y.; Deng, Z. γ-Fe2O3 nanoparticles embedded in porous carbon fibers as binder-free anodes for high-performance lithium and sodium ion batteries. *J. Alloy. Compd.* **2019**, *777*, 127–134.
13. Narsimulu; D.; Nagaraju; G.; Sekhar; S.C.; Ramulu; B.; Yu, J.S. Three-dimensional porous SnO2/carbon cloth electrodes for high-performance lithium-and sodium-ion batteries. *Appl. Surf. Sci.* **2021**, *538*, 148033.
14. Tang; C.; Zhang; H.; Jiao; D.; Hu; R.; Liu, Z. Hierarchical C-doped CuO nanorods on carbon cloth as flexible binder-free anode for lithium storage. *Mater. Des.* **2019**, *162*, 52–59.
15. Wang; D.; Wang; Y.; Li; Q.; Guo; W.; Zhang; F.; Niu, Urchin-like α-Fe2O3/MnO2 hierarchical hollow composite microspheres as lithium-ion battery anodes. *J. Power Sources* **2018**, *393*, 186–192.
16. Wang; S.-G.; Lin; J.; Fan; C.-Y.; Li; Y.-F.; Zhang; J.-P.; Wu; X.-L.; Sun; H.-Z.; Deng; M.-X.; Su, Z.-M. Target encapsulating NiMoO4 nanocrystals into 1D carbon nanofibers as free-standing anode material for lithium-ion batteries with enhanced cycle performance. *J. Alloy. Compd.* **2020**, *830*, 154648.
17. T.-F.; Peng; P.-P.; Han; X.; Zhu; Y.-R.; Luo, S. Interconnected Co3O4@CoNiO2@PPy nanorod and nanosheet composite grown on nickel foam as binder-free electrodes for Li-ion batteries. *Solid State Ion.* **2019**, *329*, 131–139.
18. Tyagi; A.; Banerjee; S.; Cherusseri; J.; Kar, K.K. Characteristics of transition metal oxides. In *Handbook of Nanocomposite Supercapacitor Materials I; Springer:* 2020; pp. 91–123.
19. X.; Yue; J.; Li; L.; Xue; H.; Yang; J.; Zhao, X. General Synthesis of MnOx (MnO2, Mn2O3, Mn3O4, MnO) Hierarchical Microspheres as Lithium-ion Battery Anodes. *Electrochim. Acta* **2015**, *184*, 250–256.
20. J.Y.; Ji; S.; Unithrattil; S.; Lee; S.S.; Kim; Y.; Jung; H.-K.; Kang; Im, B.; W.; Choi, S. Rational design of electrochemically active polymorphic MnOx/rGO composites for Li+-rechargeable battery electrodes. *Ceram. Int.* **2019**, *45*, 9522–9528.
21. Yadav, M.S. Synthesis and characterization of Mn2O3−Mn3O4 nanoparticles and activated charcoal based nanocomposite for supercapacitor electrode application. *J. Energy Storage* **2020**, *27*, 101079.
22. Bhatt; M.D.; Lee, J.Y. High capacity conversion anodes in Li-ion batteries: A review. *Int. J. Hydrog. Energy* **2019**, *44*, 10852–10905.
23. Chen; M.; Wang; E.; Liu; Q.; Guo; X.; Chen; W.; Chou; S.-L.; Dou, S.-X. Recent progress on iron- and manganese-based anodes for sodium-ion and potassium-ion batteries. *Energy Storage Mater.* **2019**, *19*, 163–178.
24. Bach-Toledo; L.; Hryniewicz; B.M.; Marchesi; L.F.; Dall'Antonia; L.H.; Vidotti; M.; Wolfart, F. Conducting polymers and composites nanowires for energy devices: A brief review. *Mater. Sci. Energy Technol.* **2019**, *3*, 78–90.
25. Jia; B.; Chen; W.; Luo; J.; Yang; Z.; Li; L.; Guo, L. Construction of MnO_2 Artificial Leaf with Atomic Thickness as Highly Stable Battery Anodes. *Adv. Mater.* **2019**, *32*, 1906582.
26. Voskanyan; A.A.; Ho; C.-K.; Chan, K.Y. 3D δ-MnO2 nanostructure with ultralarge mesopores as high-performance lithium-ion battery anode fabricated via colloidal solution combustion synthesis. *J. Power Sources* **2019**, *421*, 162–168.
27. Abdah; M.A.A.M.; Mokhtar; M.; Khoon; L.T.; Sopian; K.; Dzulkurnain; N.A.; Ahmad; A.; Sulaiman; Y.; Bella; F.; Su'ait, M.S. Synthesis and electrochemical characterizations of poly (3, 4-ethylenedioxythiophene/manganese oxide coated on porous carbon nanofibers as a potential anode for lithium-ion batteries. *Energy Rep.* **2021**, *7*, 8677–8687.
28. Magu; T.O.; Agobi; A.U.; Hitler; L.; Dass, P.M. A Review on Conducting Polymers-Based Composites for Energy Storage Application. *J. Chem. Rev.* **2019**, *1*, 19–34.
29. Sui; Y.; Liu; C.; Zou; P.; Zhan; H.; Cui; Y.; Yang; C.; Cao, G. Polypyrrole coated δ-MnO 2 nanosheet arrays as a highly stable lithium-ion-storage anode. *Dalton Trans.* **2020**, *49*, 7903–7913.
30. Lin, Y.; Zhang, L.; Xiao, J.; Liu, H. MnO/C cubo-polyhedrons derived from α-MnO 2@ ZIF-8 as anode materials for high-performance lithium-ion batteries. *Sustain. Energy Fuels* **2020**, *4*, 633–642.
31. Cao, Z.; Yang, Y.; Qin, J.; Su, Z. A core-shell porous MnO2/Carbon nanosphere composite as the anode of lithium-ion batteries. *J. Power Sources* **2021**, *491*, 229577.
32. Zhang, X.; Su, X.; Zhang, B.; Wang, J. Preparation of MnO2@ CNFs composites and their tunable microwave absorption properties. *Mater. Res. Express* **2019**, *6*, 075005.
33. Wang, Z.; Han, Y.; Fan, W.; Wang, Y.; Huang, L. Shell-core MnO2/Carbon@ Carbon nanotubes synthesized by a facile one-pot method for peroxymonosulfate oxidation of tetracycline. *Sep. Purif. Technol.* **2021**, *278*, 119558.
34. Kim, E.S.; Lee, H.-J.; Kim, B.-H. Sandwich-structured carbon nanofiber/MnO2/carbon nanofiber composites for high-performance supercapacitor. *Electrochim. Acta* **2022**, *406*, 139883.

35. Huang, C.-L.; Chiang, L.-M.; Su, C.-A.; Li, Y.-Y. MnO2/carbon nanotube-embedded carbon nanofibers as core–shell cables for high performing asymmetric flexible supercapacitors. *J. Ind. Eng. Chem.* **2021**, *103*, 142–153.
36. Cui, Y.; Yang, K.; Lyu, Y.; Liu, P.; Zhang, Q.; Zhang, B. Hollow nitrogen-doped carbon nanofibers filled with MnO2 nanoparticles/nanosheets as high-performance microwave absorbing materials. *Carbon* **2022**, *196*, 49–58.
37. Dirican, M.; Yanilmaz, M.; Asiri, A.M.; Zhang, X. Polyaniline/MnO2/porous carbon nanofiber electrodes for supercapacitors. *J. Electroanal. Chem.* **2020**, *861*, 113995.
38. Park, J.H.; Choi, W.Y.; Lee, S.; Kim, T.-S.; Lee, J.W. Graphene intercalated free-standing carbon paper coated with MnO2 for anode materials of lithium ion batteries. *Electrochim. Acta* **2020**, *348*, 136310.
39. Zhao, Y.; Chang, L.; He, W.; Xu, S.; Liu, K.; Huang, T.; Li, Y.; Cui, M.; Xie, J. Improved supercapacitive performances of manganese dioxide on acid-treated carbon nanofibers derived from polyaniline. *J. Energy Storage* **2023**, *60*, 106596.
40. Yan, S.; Tang, C.; Wang, X.; Zhang, H.; Yang, Z.; Zhang, C.; Liu, S. Hierarchical MnO2 nanowire arrays consisting of multitripod structures grown on porous carbon nanofibers for high-performance supercapacitor electrode. *J. Electroanal. Chem.* **2020**, *856*, 113475.
41. Jeong, J.H.; Kim, Y.A.; Kim, B.-H. Electrospun polyacrylonitrile/cyclodextrin-derived hierarchical porous carbon nanofiber/MnO2 composites for supercapacitor applications. *Carbon* **2020**, *164*, 296–304.
42. Liu, C.-S.; Huang, C.-L.; Fang, H.-C.; Hung, K.-Y.; Su, C.-A.; Li, Y.-Y. MnO2-based carbon nanofiber cable for supercapacitor applications. *J. Energy Storage* **2021**, *33*, 102130.
43. Rao, T.P.; Kumar, A.; Naik, V.M.; Naik, R. Effect of carbon nanofibers on electrode performance of symmetric supercapcitors with composite α-MnO2 nanorods. *J. Alloys Compd.* **2019**, *789*, 518–527.